Molecular Dynamics Simulations of the Enzyme Cu, Zn Superoxide Dismutase

Ricardo J. F. Branco, Pedro A. Fernandes, and Maria J. Ramos*

REQUIMTE, Departamento de Química, Faculdade de Ciências, Universidade do Porto, Rua do Campo Alegre, 687, 4169-007 Porto, Portugal

Received: November 25, 2005; In Final Form: April 26, 2006

The enzyme Cu, Zn superoxide dismutase (Cu,Zn-SOD) is a ubiquitous oxireductase, which is responsible for the cellular defense against oxidative stress caused by the high toxicity of the superoxide radical, and has been also linked to some cases of familiar amyotrophic lateral sclerosis. In the present study a set of molecular mechanics parameters for the active site of Cu,Zn−SOD has been derived. Afterward, an extensive molecular dynamics simulation has been carried out in an aqueous environment. The obtained results shed a further light on the structural flexibility of the backbone, where the active site is nested, and the solvation shell occupancy. The relatively small backbone deviation, shown by a root-mean-square deviation below 1.0 Å, confirms the accuracy of the parameters. The solvent shell analysis has shown that the first solvation shell is located at about 5 Å from the copper ion, generating an empty cavity with enough space to accommodate the superoxide radical. The low residence time means that a high permutation rate of water molecules in both solvation shells is consistent with the efficiency of this catalytic mechanism. Hybrid studies using ONIOM methodologies can now be done to evaluate the mechanistic implications of the explicit inclusion of the whole system.

Introduction

Copper, zinc superoxide dismutase (Cu,Zn-SOD) is a homodimeric metalloenzyme, which is responsible for the cellular defense against oxidative damage, caused by the high toxicity of the superoxide radical ($O_2^{\bullet-}$) released during respiration, photosynthesis, or as a consequence of an immune system response. Each subunit contains a bimetallic center with one copper, Cu(II), and one zinc ion, Zn(II), bridged by the histidinate ring of the His61 residue (amino acid sequence numbered according to the bovine erythrocyte structure). Only the copper ion is directly involved in the catalytic mechanism.[1] The zinc ion is buried in the protein and has mainly a structural role.[2]

There are three more classes of SODs in nature, with different metal ion contents: Fe-SOD, mainly found in prokaryotes,[3] Mn-SOD, also found in the matrix of mitochondria,[4] and the recently discovered Ni-SOD.[5] The widely accepted catalytic mechanism[1] comprises two steps. In the first one the Cu^{2+} is reduced to Cu^{+}, with the concomitant oxidation of the $O_2^{\bullet-}$ to molecular oxygen (O_2). Simultaneously, the Cu−His61−Zn bridge is broken and the His61 Nϵ2 atom is protonated. In the second step the tricoordinated cuprous ion is reoxidized to the initial form by another $O_2^{\bullet-}$, and the copper ion regains its characteristic distorted square planar geometry, with the release of a hydrogen peroxide molecule (H_2O_2) and reforming of the His61 bridge between Cu and Zn. The well-ordered conserved network of water molecules in the active site channel is suggested to be the source of the proton for His61[6] required for the dismutation.

The high catalytic rate of Cu,Zn-SOD (about $(2-3) \times 10^9$ M^{-1} s^{-1} at 298 K[7,8]), when compared with the spontaneous dismutation (about 2×10^5 M^{-1} s^{-1} at physiological pH[4]), can be justified by some unusual electrostatic and structural features. To make the reaction thermodynamically efficient it is essential to keep the redox potential of Cu,Zn-SOD between the values of $E^{\circ\prime}(O_2/O_2^{\bullet-}) = -160$mV and $E^{\circ\prime}(O_2^{\bullet-}/H_2O_2) = +890$mV ($E^{\circ\prime}$ values are given vs the standard hydrogen electrode), although the standard reduction potential of the aqua ion $Cu(H_2O)_n^{+/2+}$ is 0.16 V.[9] Thus, the nature, number, and geometry of ligands around the metal ion should be tuned to fit these requirements. Furthermore, the protein also has to provide specific interactions to drive and bind the $O_2^{\bullet-}$ during the entrance to the active site channel. Other protein functions include to ensure available hydrogen donor/acceptor residues near the metal site, to assist the catalysis, and to keep the active site structure in a favorable distorted geometry. Arg141 and Thr151 have been proposed to play an important role, being responsible for the local electrostatic attraction of the substrate.[10] Some other conserved residues, such as Lys120, Asp130, Glu131, and Lys134, are responsible for the electrostatic driving of the superoxide radical along the active site access channel.[11]

Some theoretical studies have shown that the potential energy surface associated with geometrical changes in the copper coordination sphere that occur upon reduction/reoxidation of the copper ion is fairly flat.[12] This suggests that the exchange at the fifth position on the copper coordination shell upon substrate binding, commonly described in the literature as initially occupied by a loosely coordinated water molecule, is easy, contributing to an increase in the efficiency of the catalytic process. Water molecules on the active site channel are responsible for the stabilization of important residues such as Arg141 and Thr135, constitute the main source of protons,[7] and also permit large-amplitude fluctuations of the side chains and loops forming the protein active site required to facilitate the diffusion of substrate and products to and from the catalytic center.[13]

The study of the catalytic mechanism of this enzyme by hybrid quantum mechanical/molecular mechanical (QM/MM)

* Author to whom correspondence should be addressed. Phone: (+351) 22 608 28 26. E-mail: mjramos@fc.up.pt.

10.1021/jp056855l CCC: $33.50
Published on Web 07/29/2006

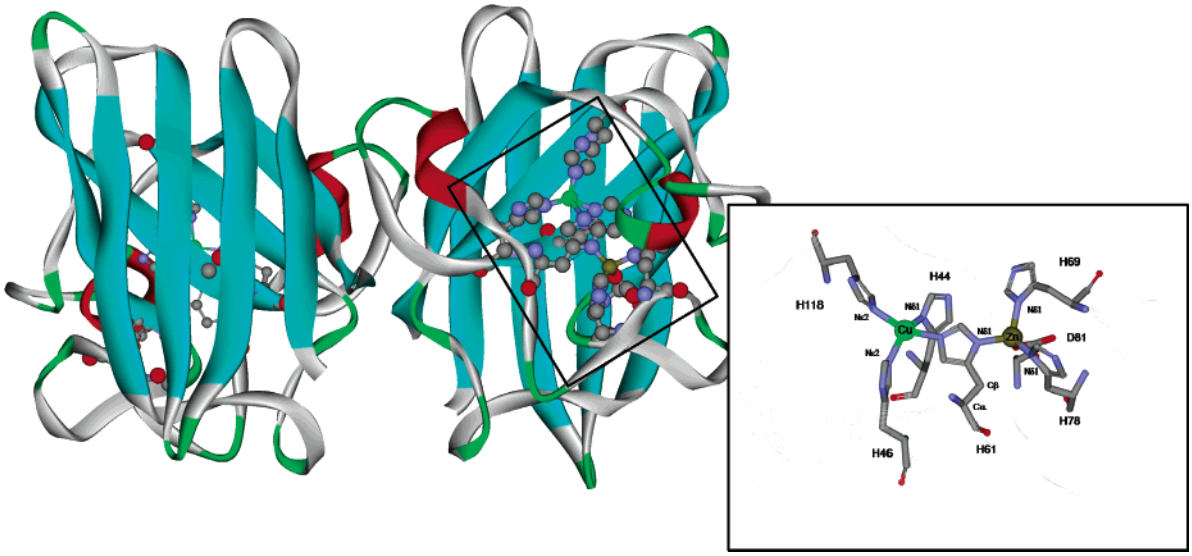

Figure 1. Model of the active site of Cu,Zn-SOD, taken from PDB code 1CBJ, used in the DFT calculations. The atomistic structure is colored by atom type (dark gray, C; light blue, N; red, O), and amino acids are displayed as balls and sticks and metal ions as CPK models. The backbone of the protein is represented as a ribbon.

methods such as ONIOM requires force fields parameters for all intra- and intermolecular interactions. Unfortunately, in this particular case they are not defined for metallic ions of the active site, and then they have to be derived. We have derived a set of MM parameters for bonds and angles, as well as atomic charges, for the Cu and Zn ligands of the active site, which are consistent with the AMBER force field,[14] and performed extensive molecular dynamics simulations, which provided information about the structural features of the active site. With these parameters it is also possible to reproduce the characteristic tetrahedral distortion of the active site as well as analyze the solvation shell occupancy at the active site of the enzyme.

Computational Methods

All calculations were performed on the crystallographic structure of bovine Cu,Zn-SOD, with 1.65 Å resolution (with PDB code 1CBJ),[6] from the Protein Data Bank.[15] The global formal charge of the protein was neutralized by the addition of 4 Na^+ counterions. The 18 missing atoms in the crystal structure (chain A, Lys 3, 9, and 89; chain B, Lys 89 and 134; atom types, CD, CE, NZ, and CG of Lys 89 in chain B) and the corresponding hydrogen atoms were added. Afterward the structure was solvated with a cubic box of water molecules described by the TIP3P force field parameters and geometry[16] with a minimal distance of 12 Å between the wall and the enzyme, totaling 44 119 atoms. All these steps were done using the xLEAP module of the AMBER software package.[17]

Parameter Set Derivation. Atomic charges, force constants for bonds and angles, and equilibrium bond and angle values, for the active site of the Cu,Zn-SOD, were derived entirely from quantum mechanics calculations, using the Gaussian 03 software package.[18] Parameters for all other residues were found in the AMBER force field. In this force field the total energy of the system is modeled by the potential function shown in the following equation, where K_r and K_θ are the harmonic potential constants for bonds and valence angles, V_n is the torsional potential constant for dihedral angles, r is the bond length, r_{eq} is the equilibrium bond length, θ is the valence angle, θ_{eq} is the equilibrium angle value, ϕ is the dihedral angle value, n is the periodicity, q_i and q_j are the atomic charges, ϵ is the effective dielectric constant, and R_{ij} is the distance between the atoms. The nonbonded term, calculated for atoms separated by at least three chemical bonds, is modeled using a Lennard-Jones potential for van der Waals interactions and a Coulomb potential term for the electrostatic interactions

$$U(R) = \sum_{\text{bonds}} K_r(r - r_{\text{eq.}})^2 + \sum_{\text{angles}} K_\theta(\theta - \theta_{\text{eq.}})^2 + \sum_{\text{dihedrals}} \frac{V_n}{2}(1 + \cos[n\phi - \gamma]) + \sum_{i<j}^{\text{atoms}} \frac{A_{ij}}{R_{ij}^{12}} - \frac{B_{ij}}{R_{ij}^{6}} + \sum_{i<j}^{\text{atoms}} \frac{q_i q_j}{\epsilon R_{ij}} \quad (1)$$

Density functional theory geometry optimizations were performed on a model of the active site comprising the copper and zinc ions and respective ligands, as shown in Figure 1, in a total of 72 and 46 atoms, respectively. Asp and His residues were modeled as formate and neutral imidazole rings, respectively,[19] resulting in a system with the formula $\{[His]_3Cu[His]\text{-}Zn[His]_2Asp\}^{2+}$. The former was truncated at the C^α atom, and the latter at the C^β atom. Density functional theory (DFT), at the unrestricted level, using the hybrid B3LYP functional[20−23] and the quasi-relativistic compact effective potentials CEP-31G basis set,[24,25] were used for all atoms as implemented in Gaussian 03.[18] This level of theory and type of basis set have been shown to be adequate to deal with the present system.[26] First, the crystallographic structure was optimized in the gas phase, with the copper and zinc ions in the oxidized form. Afterward, the potential energy surface (PES) for bond distances and angles were done assuming a rigid framework, where only the coordinates of one ligand were optimized, while all other coordinates were kept frozen.[27] Finally, equilibrium bond distances and angles and the corresponding stretching and bending force constants have been adjusted to these PES scans, assuming that each parameter is independent of all the others. This approach is the basis of the general equation used in the AMBER force field given in eq 1, which does not include cross-terms. The resulting values are compiled in Tables 1 and 2.

Charge withdrawing and donating effects are important to correctly determine the atomic point charges for the residues of the active site. Therefore, charges were calculated on a larger model of 101 atoms comprising all ligands of the copper and

TABLE 1: Metal−Ligand Bonding Parameters

bond	atom type	k_r (kcal mol^{-1} Å^{-2})	r_{eq} (Å)
Cu(II)−His Nϵ2	Cu−NB	101.1	2.022
Zn(II)−His Nδ1	Zn−NB	96.7	2.046
Zn(II)−Asp O	Zn−OS	92.0	1.949

TABLE 2: Metal−Ligand Angular Parameters

angle	atom type	k_θ (kcal mol^{-1} rad^{-2})	θ_{eq} (deg)
His Nϵ2−Cu(II)− His Nϵ2	NB−Cu−NB	24.6	147.19
His Nδ1−Zn(II)−His Nδ1	NB−Zn−NB	44.0	113.53
His Nδ1−Zn(II)−Asp O	NB−Zn−OS	21.7	111.75

zinc ions, truncated on the C^α atom. The all-electron 6-311+G (3df,3pd)[28] basis set for the Cu and Zn ions and the 6-31G basis set for the remaining atoms were used in a single-point energy calculation. The geometry of the model used to calculate the electrostatic potential (ESP) was previously optimized, keeping all C^α atoms fixed, with the aim of conserving the conformation of the active site as in the crystallographic structure and consequently eliminating possible fluctuations on the point charges due to structural relaxation.

Several methods have been tested to calculate the point charges: Mulliken population analysis,[29] where the electronic density is distributed according to the atomic orbital occupancy, and the restrained electrostatic potential (RESP) model.[30] This method estimates point charges based on a least-squares fit of the potential generated by them and on the quantum mechanics ESP but with the inclusion of hyperbolic restraints on non-hydrogen atoms, with the aim of reducing the charges on buried atoms without affecting the fit. We have tested also the CHELPG method,[31] which is similar to the RESP method, but the points are sampled on a regularly spaced cubic grid (~0.3 Å between points). The obtained results are compiled in Table 1 of the Supporting Information.

Molecular Dynamics Simulation. The energy of the system was initially minimized to eliminate any close van der Waals contacts in the structure caused by the addition of the box of water molecules, and subsequently a molecular dynamics simulation was performed.

In the molecular dynamics simulation, the SHAKE algorithm was used for all bonds involving hydrogen atoms.[32] The equations of motion were integrated with a time step of 2.0 fs. The Langevin dynamics was used with the collision frequency γ equal to 1.0 ps^{-1}, the particle mesh Ewald (PME) method was employed for the treatment of long-range electrostatic interactions, and a distance cutoff of 10 Å was used for all nonbonded interactions.

The energy-minimized system was first slowly heated from 0.0 to 300.0 K in 20 ps, with periodic boundary conditions, until the system is close to the final temperature, using the Berendsen thermostat weak-coupling method.[33] A weak harmonic constraint, with a potential force constant of 10.0 kcal/mol, was applied to the whole system to avoid large motions of the structure before the temperature was equilibrated. Then the constant pressure was turned on, and the simulation was changed to an isobaric−isothermal NPT ensemble. The density equilibration was done in the next 100 ps run. These conditions were conserved during the simulation, using a pressure relaxation time of 2.0 ps. This NPT ensemble simulation was carried out at 300 K and 1 atm, using the Berendsen thermostat and barostat.[33] The total length of the MD simulation was 1.72 ns.

The commonly used *bonded model* assumes covalent bonds between metallic centers and their ligands to keep the structural geometry of the active site conserved during simulations.[34,35] Thus it was assumed that the bridge histidine (His61) was not protonated during the simulation, and it had a formal net charge of −1, as can be seen in Figure 2, residue HIG.

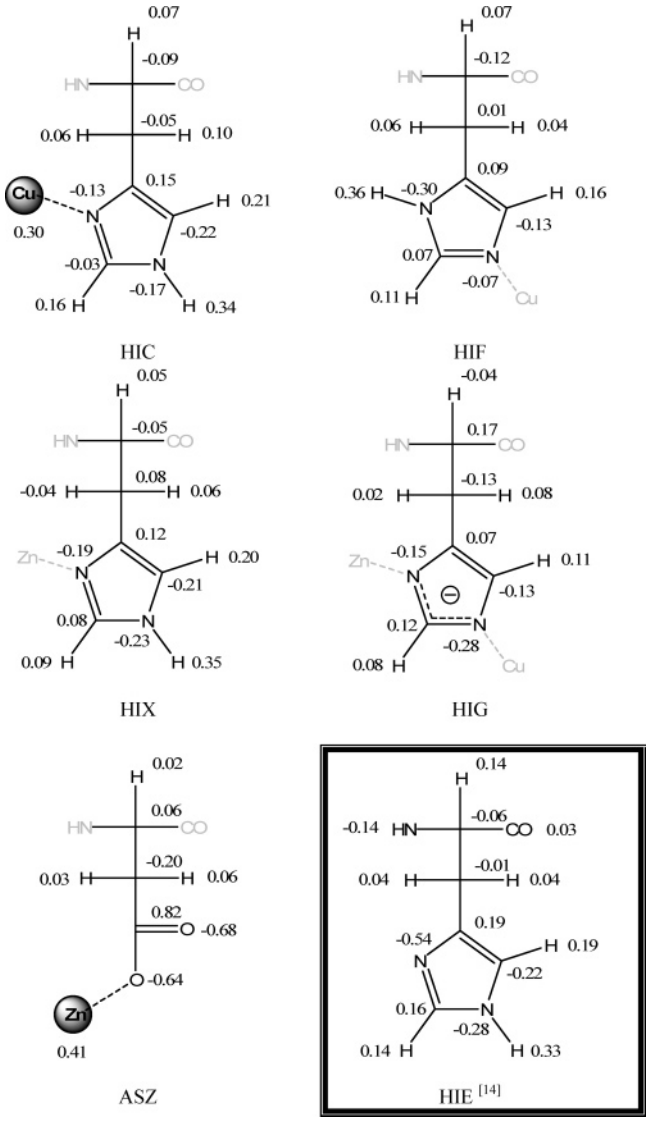

Figure 2. Atomic charges for parametrized residues calculated with the CHELPG method.

Results and Discussion

The rigid harmonic potential surface scan has been used for the parametrization of blue copper proteins (BCPs) (type I)[27] and metallo-β-lactamases (MBLs).[36] Although both classes of proteins have a different active site motif ($Cu(His)_2CysMet$ for the BCPs and $(His)_3Zn{\cdot}HO{\cdot}ZnHisCysAsp$ for the MBLs), we can use these values as a reference, being aware of the differences in the metal ion coordination and in the level of theory used on the QM calculations (B3LYP/6-31G* for S, C, N, and H and LANL2DZ for Cu in the case of BCP and HF/6-31G* in the case of MBL). All force field parameters for the copper and zinc ions and theirs ligands in Cu,Zn-SOD are shown in Tables 1 and 2.

The equilibrium value obtained for the Cu−His bond of 2.022 Å seems to be in good agreement with the value of 2.067 Å derived by Comba et al. for BCPs,[27] using the same functional, B3LYP, and the standard LANL2DZ effective core potential basis set for copper instead of CEP-31G.[25] The difference

TABLE 3: Average Bond Lengths Calculated during the MD Simulation and in the Crystallographic Structure[a]

	X-ray 1CBJ[6] (1.65 Å)		X-ray 1Q0E[39] fully reduced (1.15 Å)		MD simulation (standard deviation 0.06 Å)	
metal−ligand	A	B	A	B	A	B
Cu−His44δ1	2.07	2.00	2.02	2.05	2.03	2.04
Cu−His46Nϵ2	2.00	2.17	1.96	2.01	2.08	2.07
Cu−His61Nϵ2	(3.19)[b]	2.20	(3.39)[b]	(3.32)[b]	2.03	2.03
Cu−His118Nϵ2	2.03	2.19	2.08	2.04	2.03	2.03
Zn−His61Nδ1	1.97	2.02	2.05	2.05	2.03	2.03
Zn−His69Nδ1	2.03	2.07	2.05	2.05	2.05	2.04
Zn−His78Nδ1	2.07	1.75	2.06	2.06	2.06	2.05
Zn−Asp81OS	1.62	1.84	1.99	2.00	1.90	1.92

[a] A and B are used to differentiate the two subunits of the enzyme. All distances are in angstroms. [b] Corresponding to the ligand that is not bound to the metal ion in the reduced state.

between the Cu−His stretching force constant in Cu,Zn-SOD and in BCP is about 30 kcal mol^{-1} Å^{-2} (101.1 and 131.5 kcal mol^{-1} Å^{-2}, respectively), which is probably due to the nature of the ligand environment in both copper complexes as well as due to the difference in the theoretical level used. In BCP, as the equilibrium distances Met−Cu and Cys−Cu are longer than the His−Cu distance (2.700, 2.230, and 2.067 Å respectively), the two histidines are tightly bound to the metal ion, probably due to a better orbital overlapping, which strengthens the bond between metal ion and ligand. It is also well-known that SOD's active site has a distorted quadrangular planar geometry,[26] and therefore it is expected that the equilibrium angle would be higher in SOD than in BCP, 147.19° versus 103.00°, even though the corresponding force constants are very similar, 24.6 versus 22.0 kcal mol^{-1} rad^{-2}. The characteristic geometry of BCPs is closer to trigonal pyramidal, in which both histidine residues are in the same plane of the copper.

Parameters for the zinc center were derived in the same way as those for copper, and their values can be compared with the MBL ones. Although the Zn−His equilibrium bond length of 2.046 Å and respective force constant 96.7 kcal mol^{-1} Å^{-2} are in good agreement with 2.070 Å and 103.0 kcal mol^{-1} Å^{-2} for the MBL,[36] the equilibrium angle and the bending force constant of 113.53° and 44.0 kcal mol^{-1} rad^{-2} are higher than the values of 105.00° and 20.0 kcal mol^{-1} rad^{-2} found in the MBL enzymes. These parameters were derived with a lower level of theory, HF/6-31G*. Part of the difference can be ascribed to the improvement in the level of theory, since in the Hartree−Fock (HF) method an additional inaccuracy stems from the neglect of electron correlation.

Considering the arguments used before to justify the difference between the calculated parameters for the Cu−His bond in this system and in systems in which the His residues are replaced by Cys or Met, it can be expected that a similar effect occurs with Zn−Asp parameters, since the dinuclear zinc β-lactamase site motif has HisCysAsp·H_2O ligands instead of His_3Asp as in SOD. The equilibrium bond length of 1.949 Å and the equilibrium bond angle of 111.75° are in agreement with the values of 1.970 Å and 105.00° for MBL. However, the stretching force constant of 92.0 kcal mol^{-1} Å^{-2} is about 40 kcal mol^{-1} Å^{-2} less than the value reported for MBL of 134.0 kcal mol^{-1} Å^{-2}. The bending force constant is very sensitive to small conformational changes, and the value can range between 40.0 and 80.0 kcal mol^{-1} Å^{-2} for the Zn−Asp bond, considering two different conformations in the MBL Zn site; the calculated parameter of 21.7 kcal mol^{-1} rad^{-2} for Cu,Zn-SOD is therefore plausible.[36] The harmonic bond and angle potential curves are appended in the Supporting Information. To avoid problems of anharmonicity, the curve fitting was adjusted to the PES considering only the points with a ΔE inferior to 3 kcal/mol for the bond stretching and about 10 kcal/mol for the angle bending.

The differences among point charges calculated according to different approaches are discussed in detail here, and the complete results are compiled in the Supporting Information. It is important to be aware that buried atoms, mainly metal ions such as Cu^{2+} or Zn^{2+}, can be overestimated or underestimated by some of these methods quite easily if grid sampling is not accurately chosen. The point charge in the metal ion should reflect the charge transferred to the ligands, and therefore the real value is expected to be considerably lower than their formal charge of +2. Point charge descriptions for the BCP active site have been reported in the literature, in which the copper has a value near 0.33 au, using the Merz−Singh−Kollman scheme.[27] The zinc ion in MBL enzymes has a slightly higher value, about 0.50 au, taken from 6-31G* ESP calculations.[37]

From the results it is clear that the Mulliken point charges for the majority of atoms are higher than those of other methods, as predicted.[38] This method, as mentioned before, does not take into account differences between atoms and consequently splits the electronic density among them, based on orbital occupancy. The most common method used to derive charges, RESP, is also not able to address reasonable charge values for some atoms, unless the initial guess potentials are sampled according to a method like CHELPG, as presented in Figure 2, and in this case the values are much better. According to the CHELPG method, all C^{α} atoms are predicted to be positive, ranging between 0.22 and 0.27 au for His and 0.40 au for Asp residues, and reference values from the AMBER force field range from −0.06 to 0.02 au and 0.04 au, respectively. The values for the metal ions, 0.27 au for copper and 0.30 au for zinc, are in good agreement with values reported previously (0.33 and 0.50, au respectively).[27,36] These were the values chosen for the MD simulation.

Average metal−ligand bond lengths were compared with the corresponding crystallographic values to evaluate their accuracy over the simulation. The results are compiled in Table 3, which summarizes the information of the graphics appended in the Supporting Information.

The average bond distances between metal ions and ligands over the simulation show a low standard deviation (<0.060 Å) for all ligands and a great accordance in comparison to the metal ligand bond distance in both subunits (a difference of less than 0.012 Å). It is interesting to see that the Nϵ2 of His 61 comes from a distance of 3.19 Å in the starting crystallographic structure to reach an average distance of 2.026 Å, which is almost equal in subunit B (2.027 Å). This fact shows that parameters are able to convert accurately a reduced into an oxidized active site with the correct structural characteristics. The generally accepted catalytic mechanism suggests that the

TABLE 4: Average Angles (deg) Calculated during the MD Simulation and in the Crystallographic Structure

	X-ray 1CBJ (1.65 Å)		MD simulation (standard devation 5°)	
metal−ligand	A	B	A	B
His44−Cu−His46	140.9	138.2	133.0	133.8
His44−Cu−His61	72.5	86.8	96.6	97.3
His44−Cu−His118	101.1	93.0	98.7	98.0
His46−Cu−His61	92.5	97.6	101.2	101.5
His46−Cu−His118	117.6	99.7	107.5	106.6
His61−Cu−His118	118.5	153.9	121.6	121.4
His61−Zn−His69	108.1	110.0	106.5	105.1
His61−Zn−His78	110.0	110.2	106.7	106.3
His61−Zn−Asp81	104.6	103.9	111.4	112.4
His69−Zn−His78	118.9	117.3	112.8	112.9
His69−Zn−Asp81	98.0	99.7	105.3	103.8
His78−Zn−Asp81	115.9	114.5	113.4	115.5

TABLE 5: Average Twist Angle (deg) between the Planes Defined by the Three Atoms in the Coordination Shell of Metal Ion, Calculated during the MD Simulation and in the Crystallographic Structure

	X-ray 1CBJ (1.65 Å)		MD simulation (standard deviation 4°)	
	A	B	A	B
Cu Site	−60.30	−44.70	−58.31	−58.29
Zn Site	−63.70	−64.70	−70.16	−70.11

imidazole ring of His61 rotates about 20° upon copper reduction and turns back to the initial position in the second step of the mechanism.[6] The coherence among results validates our approach of considering a high-resolution structure as a starting model, even though without the same oxidation state in both subunits. We observed that only the His61 residue and copper ion are reoriented, as proposed by the widely accepted mechanism,[1] and at the end of simulation the structures of both subunits converged to the typical conformation of the oxidate state, keeping the remaining ligands almost in the initial geometry.

The comparison of the calculated average distances for each ligand−metal with the corresponding crystallographic values should be done, taking into account the discrepancy between the values obtained from two X-ray structures (PDB codes 1CBJ and 1Q0E). The values from the 1.65 Å X-ray structure are substantially different when compared with the values from the 1.15 Å X-ray structure, especially in the A subunits, which are in the same redox state. The difference for each ligand is less than 0.09 Å, when compared with the values from the 1.15 Å X-ray structure, which demonstrates the quality of the parameters.

The analysis of the angle between the active side ligands is compiled in Table 4.

With exception of the His61−Cu−His118 in subunit B, the remaining angles reported here are in good agreement with the values taken from the crystallographic structure. The difference between the experimental and the theoretical values is less than 11° for almost all pairs of ligands. The angle His44−Cu−His61 in subunit A changes more than 20°, during the simulation, and approaches the value found in subunit B for the same ligand pair whereas the angle His61−Cu−His118 in subunit B varies about 30°. The global active site geometry stands between a planar geometry, in which all angles are equal to 120°, and a tetrahedral geometry characterized by angles of 109.5° between the ligands.

The twist angle ϕ[40] (Figure 3) was calculated for copper and zinc sites in both subunits of the enzyme as being −58°. This

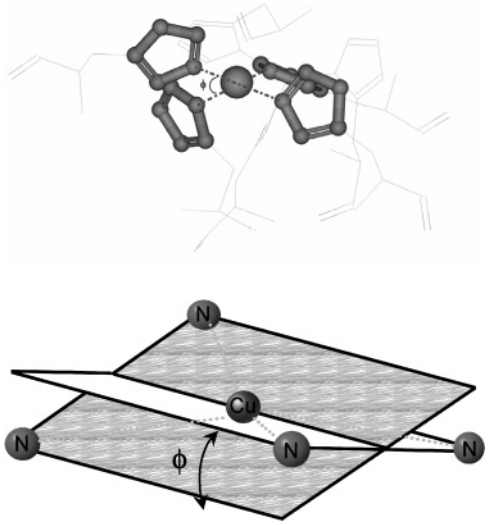

Figure 3. Twist angle ϕ between the planes defined by the nitrogen atoms coordinated to the copper ion in the active site of the Cu,Zn-SOD enzyme.

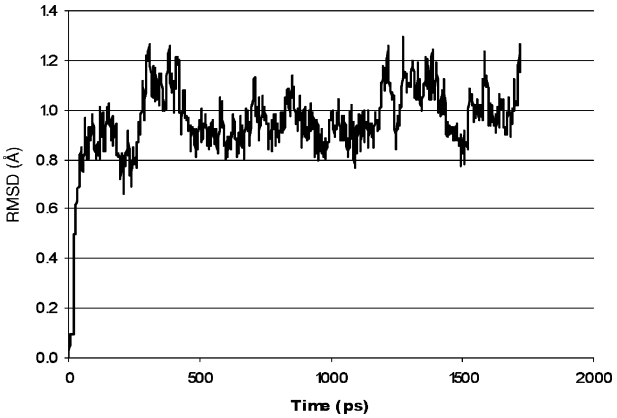

Figure 4. Root-mean-square deviation (Å) between the crystallographic structure and each frame of the MD simulation.

is in good agreement with the range of experimental values, −60° for subunit A and −45° for subunit B, Table 5. The smooth asymmetry between two subunits in the crystallographic structure is due to the different redox state of each subunit. The ϕ value is crucial to evaluate the accuracy of force field parameters, since we believe that the backbone of the protein is implicated in the maintenance of this angle in a narrow interval to maximize the catalytic efficiency of the enzyme. However one should be aware that ϕ is neither a strong nor a direct proof of the force field's quality.[41]

Another essential value widely used to validate parameter sets is the root-mean-square deviation (RMSD). In this simulation the backbone atoms' RMSD, relative to the first structure, was 0.95 ± 0.15 Å. Thus, as shown in Figure 4, the deviation from the starting X-ray coordinates was very small during the course of the simulation. This means that the structure is mainly conserved over the MD simulation, and then we can conclude, based on structural data shown here, that the structural changes are not significant and the force field is accurately parametrized for this enzyme.

Solvation Shell Analysis. The radial distribution function (RDF) analysis (Figure 5) shows that only zinc ion (part B) has a defined first solvation shell with two molecules of water located in a radius of 4 Å. The copper ion does not have a first solvation shell and has only a second solvation shell, located at

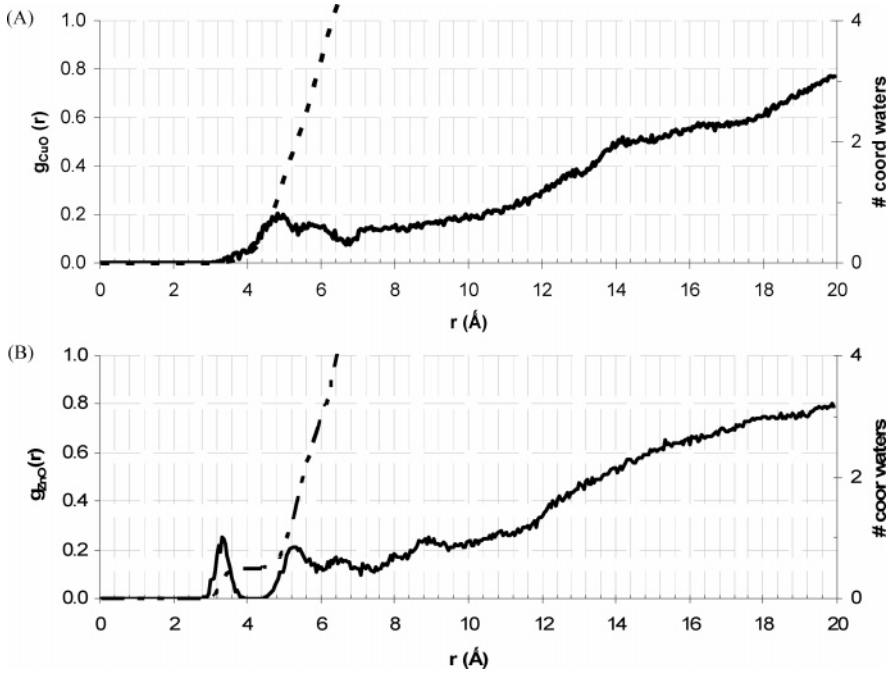

Figure 5. RDFs obtained from the solvent shells during the MD simulation for (A) copper and (B) zinc ion, respectively.

4−7 Å from it. Afterward the RDF value increases until it reaches the bulk value, where the RDF equals unity.

This is indeed a very important finding resulting from the MD simulations that can provide new, interesting insights concerning the role of water in the mechanism of SOD. We have conducted a full search of the PDB, located a total of 182 subunits presenting the three-dimensional geometries for SOD (Supporting Information), and classified them in terms of the solvation sphere to which they belong.

From the copper−oxygen RDFs in bulk water (Schwenk and Rode,[42] Figure 1 of the Supporting Information), we see that the first peak is located at 2.02 Å and that the probability for the presence of water is basically zero after 2.60 Å, until the appearance of the peak corresponding to the second solvation shell, centered at 4.13 Å.

Additionally, there are also other studies in the literature that report on the RDF of the Cu(II) ion in aqueous solution (Rode et al.,[43] Blumberger et al.[44]). All these data seem to point to the fact that for a water molecule to be coordinated to the Cu(II) ion, in what can be designated as a first coordination sphere, the Cu−O distance must be around 2 Å. This is certainly notwhat our simulations indicate, and rather there is a very loosely coordinated water molecule at a distance that can hardly be considered a first solvation sphere.

Taking these values as a reference, we have classified the closest water molecules in the PDB files as belonging to the first solvation shell (distances lower than 2.60 Å), to the region between first and second solvation shells (distances between 2.60 and 3.40 Å), and to the second solvation shell (distances larger than 3.40 Å).

We concluded that there is not a single structure that has a water in a pure first solvation shell (Cu−O ≈ 2 Å) and the closest water molecules that can be found are always in the periphery of the first solvation shell. (The mean distance of the 31 subunits (17% of all subunits) that have a water molecule within a distance of 2.60 Å of the Cu ion is equal to 2.30 Å.) However, there are 73 subunits, which represent 40% of the total of subunits, that do not have any water molecule in the first coordination shell. A total of 47 structures (26%) have a water molecule in the gap between the first and the second

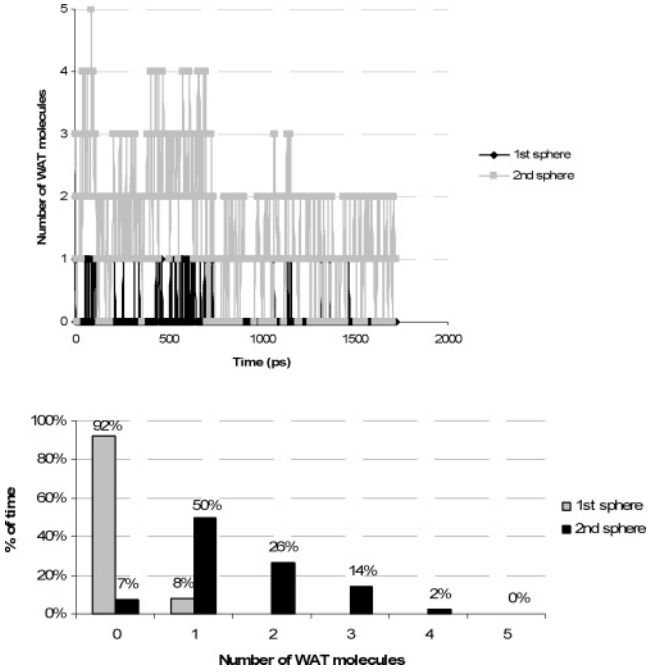

Figure 6. Time evolution of water molecules in the first and second solvation shell of the copper ion and average composition of the solvation shells.

solvation spheres, with a mean distance of 3.06 Å, and the remaining 31 structures (17%) have the first water in the second solvation shell, with a mean distance of 3.58 Å. Therefore, already from this study, doubt remains as to whether or not there is a first solvation sphere for the Cu ion.

The analysis of the first and second solvation shell of the copper ion (Figure 6) reveals that after the first 700 ps of simulation it is only possible to locate water molecules in the second shell. It is also interesting to note that, near the simulation time of 1150 ps, the number of water molecules in the second shell momentarily increases from two to three. However, the residence times of all of them are too low to be considered as putative candidates for any hydrogen bond with catalytic interest. These quick changes in the solvation shell suggest a rapid

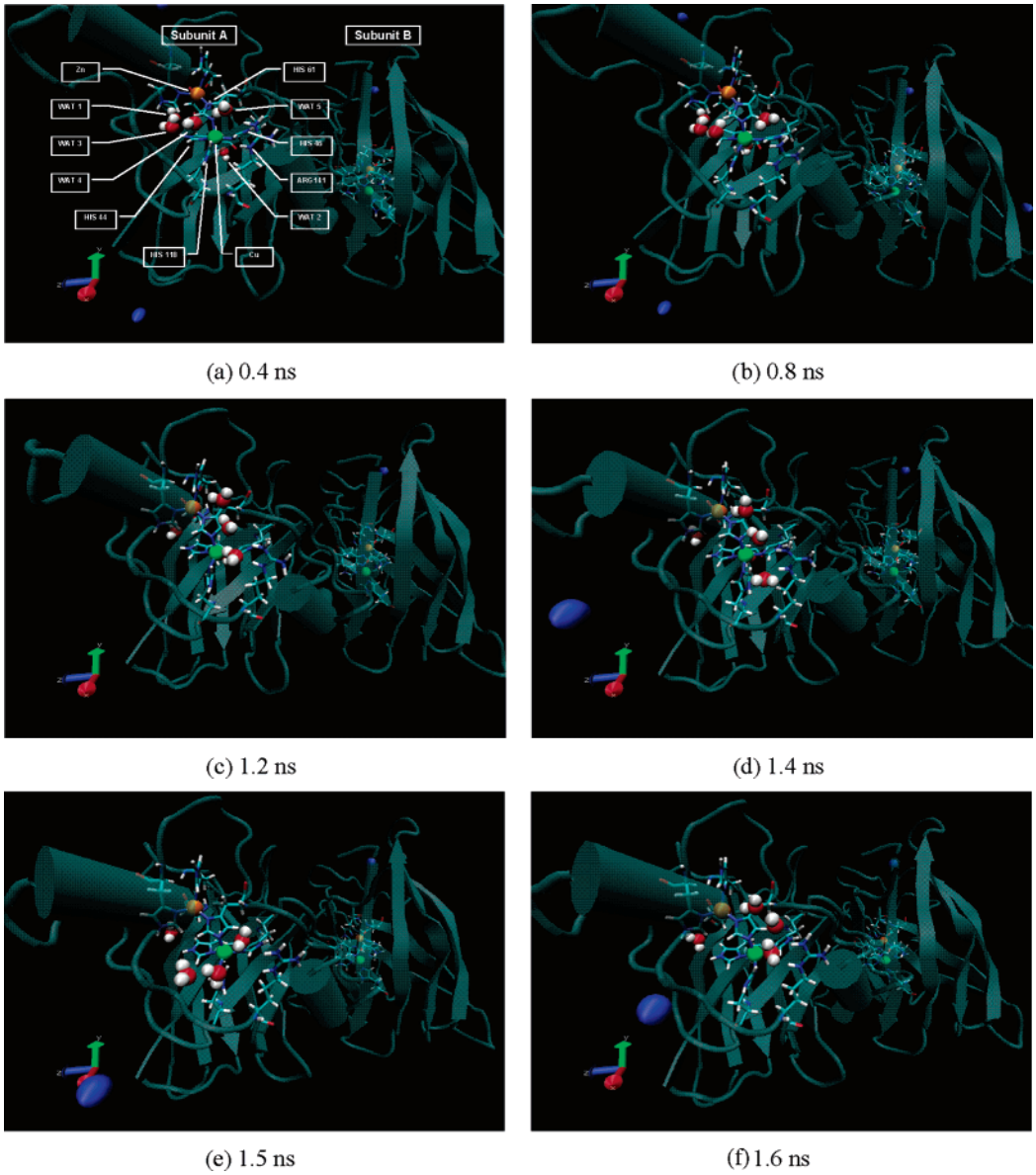

Figure 7. Configurations of the MD trajectory. The active site of subunit A and solvation shell, including the five closest waters to copper are shown. The blue CPK model represents Na^+ counterions.

permutation of the closest waters near the copper ion with the bulk solvent.

The bar graph in Figure 6 shows that only in 8% of simulation time the first solvation shell of the copper ion is occupied with one water molecule and that in the second shell it has one in 50% of the time, two water molecules 26% of the time, and three water molecules 14% of the time.

The set of snapshots shown in Figure 7 suggests that water molecules in the active site are not randomly located. We have observed in the animation of the simulation that they are almost always in two specific alignments. In the first half of the simulation they are essentially aligned along the direction parallel to the plane defined by copper's ligands at the entrance of the active site cavity. In the second half of the simulation (1.2−1.6 ns) they are essentially aligned perpendicular to the copper ligand plane. Interestingly, both configurations are in equilibrium and interchange easily on a time scale of picoseconds, as demonstrated in snapshots e and f. It is shown that there are at least two preferential regions, near to the catalytic site, that are able to nest solvent molecules. It should be interesting to analyze the solvent disposition trend in the presence of the substrate. The two remaining water molecules are buried in the protein structure, behind the copper ion. These waters (WAT1 and WAT2) are almost conserved in the same positions during the simulation, since they are located in a non-solvent-exposed region of the protein.

In the crystallographic structure WAT3, WAT4, and WAT5 are placed between the Arg141 residue and the copper ion, as in configurations taken at 0.4, 0.8, and 1.5 ns.

Some previous works[45,46] concentrate on generic conclusions on preferential hydration sites in the system without specific mention of the first solvation sphere. Others[13,47,48] focus on the specific parts of Cu,Zn-SOD, such as a single amino acid mutation at the dimer interface,[13] the effect of temperature on dimer asymmetry,[47] or structure−function relationships by site-directed mutagenesis of four conserved residues at the electrostatic loop;[48] none of these studies have results concerning the hydration of the copper ion. Additionally, there is the Banci et al. study,[49] commented upon beforehand, which states that the first shell water molecule does not leave the site (63 ps MD). Interestingly enough, the same research group in two different works[50,51] reported on the fact that in two mutants of Cu,Zn-

SOD (Ile137 mutant of the human isoenzyme, with approximately 90% of the activity of the wild-type enzyme, and the point mutant P104H, reintroducing the histidine bridging zinc and copper (His 104, corresponding to the HSOD His 63),[50] no electron density was observed for a hypothetical water molecule in the first copper coordination sphere. Furthermore, NMR dispersion measurements demonstrate the lack of a copper-coordinated water molecule on Cu,Zn-SOD from *Escherichia coli* in the oxidized Cu(II) state.[52] The authors of ref 49 state that their results suggest that, in this enzyme, the copper-coordinated water molecule appears not to be necessary for the enzymatic reaction.

Finally, in the works of McCammon et al.[53,54] the first shell water molecule does not exchange during a simulation time of 30 ps, which was demonstrated to be insufficient to see this phenomena. The RDF also has shown a second binding site for a water molecule between 3.5 and 4.5 Å from the Cu, in which water molecules do exchange several times during the simulation with other water molecules in the channel. This behavior is similar to the one that we have observed in the first 30 ps of our simulations.

Conclusions

Modeling systems that include metal centers, such as metalloproteins, is sometimes a challenge. It is essential to ensure first the accuracy of the force field to obtain a reliable structure. This is an important point and needs to be considered carefully, otherwise subsequent steps can be seriously compromised. In this work we have derived a set of MM parameters for the active site of Cu,Zn-SOD, using DFT calculations.

With the aim to validate the parameter set, we have performed molecular dynamics simulations and calculate the distances, angles, and twist angles between ligands of both metal ions, which were compared with experimental ones. The good agreement obtained between them and the relatively smooth backbone deviations, shown by a RMSD value below 1.0 Å, confirm the accuracy of the parameters.

Moreover, solvent shell analysis has been performed for both ions. The most interesting observation was that the copper ion has no first solvation shell and that the second solvation shell is placed at about 4−7 Å from the copper ion, generating an empty cavity with enough space to nest superoxide radical, without the necessity of desolvation, an obviously costly process for a divalent ion, therefore justifying the experimental observation that the catalysis kinetics is diffusion-limited.

The fact that the simulations performed in this work have shed light over a controversial fact such as the nonexistence of the first solvation sphere, suggested by spectroscopic data, is actually very important and relevant to the mechanism of SOD.

Concerning the catalytic cycle, the inexistence of a tightly bound first shell water molecule, but instead a loosely bound water molecule between the first and the second shells constitutes an important factor to allow for a high catalytic rate. It definitely facilitates the binding of the superoxide anion (remember that the enzymatic rate is diffusion-controlled), without compromising its proton-delivery role to the superoxide, which can perfectly be accomplished with the water molecule in the second shell and the superoxide in the first shell.

Supporting Information Available: Additional figures and tables. This material is available free of charge via the Internet at http://pubs.acs.org.

References and Notes

(1) Tainer, J. A.; Getzoff, E. D.; Richardson, J. S.; Richardson, D. C. *Nature* **1983**, *306*, 284−287.
(2) Bannister, J. V.; Bannister, W. H.; Rotilio, G. *CRC Crit. Rev. Biochem.* **1987**, *22*, 111−180.
(3) Battistoni, A.; Rotilio, G. *FEBS Lett.* **1995**, *374*, 199−202.
(4) Fridovich, I. *J. Biol. Chem.* **1989**, *264*, 7761−7764.
(5) Kim, E. J.; Kim, H. P.; Hah, Y. C.; Roe, J. H. *Eur. J. Biochem.* **1996**, *241*, 178−185.
(6) Hough, M. A.; Hasnain, S. S. *J. Mol. Biol.* **1999**, *287*, 579−592.
(7) Fee, J. A.; Bull, C. *J. Biol. Chem.* **1986**, *261*, 13000−13005.
(8) Fielden, E. M.; Roberts, P. B.; Bray, R. C.; Lowe, D. J.; Mautner, G. N.; Rotilio, G.; Calabres, L. *Biochem. J.* **1974**, *139*, 49−60.
(9) Holm, R. H.; Kennepohl, P.; Solomon, E. I. *Chem. Rev.* **1996**, *96*, 2239−2314.
(10) Beyer, W. F.; Fridovich, I.; Mullenbach, G. T.; Hallewell, R. *J. Biol. Chem.* **1987**, *262*, 11182−11187.
(11) Getzoff, E. D.; Tainer, J. A.; Weiner, P. K.; Kollman, P. A.; Richardson, J. S.; Richardson, D. C. *Nature* **1983**, *306*, 287−290.
(12) Noodleman, L.; Lovell, T.; Han, W. G.; Li, J.; Himo, F. *Chem. Rev.* **2004**, *104*, 459−508.
(13) Falconi, M.; Stroppolo, M. E.; Cioni, P.; Strambini, G.; Sergi, A.; Ferrario, M.; Desideri, A. *Biophys. J.* **2001**, *80*, 2556−2567.
(14) Cornell, W. D.; Cieplak, P.; Bayly, C. I.; Gould, I. R.; Merz, K. M.; Ferguson, D. M.; Spellmeyer, D. C.; Fox, T.; Caldwell, J. W.; Kollman, P. A. *J. Am. Chem. Soc.* **1995**, *117*, 5179−5197.
(15) Berman, H. M.; Westbrook, J.; Feng, Z.; Gilliland, G.; Bhat, T. N.; Weissig, H.; Shindyalov, I. N.; Bourne, P. E. *Nucleic Acids Res.* **2000**, *28*, 235−242.
(16) Jorgensen, W. L.; Chandrasekhar, J.; Madura, J. D.; Impey, R. W.; Klein, M. L. *J. Chem. Phys.* **1983**, *79*, 926−935.
(17) Case, D. A.; Darden, T. A.; Cheatham, T. E., III.; Simmerling, C. L.; Wang, J.; Duke, R. E.; Luo, R.; Merz, K. M.; Wang, B.; Pearlman, D. A.; Crowley, M.; Brozell, S.; Tsui, V.; Gohlke, H.; Mongan, J.; Hornak, V.; Cui, G.; Beroza, P.; Schafmeister, C.; Caldwell, J. W.; Ross, W. S.; Kollman, P. A. *AMBER*; University of California: San Francisco, CA, 2004.
(18) Frisch, M. J.; Trucks, G. W.; Schlegel, H. B.; Scuseria, G. E.; Robb, M. A.; Cheeseman, J. R.; Montgomery, J. A., Jr.; Vreven, T.; Kudin, K. N.; Burant, J. C.; Millam, J. M.; Iyengar, S. S.; Tomasi, J.; Barone, V.; Mennucci, B.; Cossi, M.; Scalmani, G.; Rega, N.; Petersson, G. A.; Nakatsuji, H.; Hada, M.; Ehara, M.; Toyota, K.; Fukuda, R.; Hasegawa, J.; Ishida, M.; Nakajima, T.; Honda, Y.; Kitao, O.; Nakai, H.; Klene, M.; Li, X.; Knox, J. E.; Hratchian, H. P.; Cross, J. B.; Adamo, C.; Jaramillo, J.; Gomperts, R.; Stratmann, R. E.; Yazyev, O.; Austin, A. J.; Cammi, R.; Pomelli, C.; Ochterski, J. W.; Ayala, P. Y.; Morokuma, K.; Voth, G. A.; Salvador, P.; Dannenberg, J. J.; Zakrzewski, V. G.; Dapprich, S.; Daniels, A. D.; Strain, M. C.; Farkas, O.; Malick, D. K.; Rabuck, A. D.; Raghavachari, K.; Foresman, J. B.; Ortiz, J. V.; Cui, Q.; Baboul, A. G.; Clifford, S.; Cioslowski, J.; Stefanov, B. B.; Liu, G.; Liashenko, A.; Piskorz, P.; Komaromi, I.; Martin, R. L.; Fox, D. J.; Keith, T.; Al-Laham, M. A.; Peng, C. Y.; Nanayakkara, A.; Challacombe, M.; Gill, P. M. W.; Johnson, B.; Chen, W.; Wong, M. W.; Gonzalez, C.; Pople, J. A. *Gaussian 03*; Gaussian, Inc.: Pittsburgh, PA, 2003.
(19) D'Alessandro, M.; Aschi, M.; Paci, M.; Di Nola, A.; Amadei, A. *J. Phys. Chem. B* **2004**, *108*, 16255−16260.
(20) Becke, A. D. *Phys. Rev. A* **1988**, *38*, 3098−3100.
(21) Lee, C. T.; Yang, W. T.; Parr, R. G. *Phys. Rev. B* **1988**, *37*, 785−789.
(22) Becke, A. D. *J. Chem. Phys.* **1993**, *98*, 5648−5652.
(23) Stephens, P. J.; Devlin, F. J.; Chabalowski, C. F.; Frisch, M. J. *J. Phys. Chem.* **1994**, *98*, 11623−11627.
(24) Stevens, W. J.; Basch, H.; Krauss, M. *J. Chem. Phys.* **1984**, *81*, 6026−6033.
(25) Stevens, W. J.; Krauss, M.; Basch, H.; Jasien, P. G. *Can, J. Chem.* **1992**, *70*, 612−630.
(26) Branco, R. J. F.; Fernandes, P. A.; Ramos, M. J. *J. Mol. Struct. (THEOCHEM)* **2005**, *729*, 151−156.
(27) Comba, P.; Remenyi, R. *J. Comput. Chem.* **2002**, *23*, 697−705.
(28) Frisch, M. J.; Pople, J. A.; Binkley, J. S. *J. Chem. Phys.* **1984**, *80*, 3265−3269.
(29) Mulliken, R. S. *J. Chem. Phys.* **1962**, *36*, 3428−3439.
(30) Bayly, C. I.; Cieplak, P.; Cornell, W. D.; Kollman, P. A. *J. Phys. Chem.* **1993**, *97*, 10269−10280.
(31) Breneman, C. M.; Wiberg, K. B. *J. Comput. Chem.* **1990**, *11*, 361−373.
(32) van Gunsteren, W. F.; Berendsen, H. J. C. *Mol. Phys.* **1977**, *34*, 1311−1327.
(33) Berendsen, H. J. C.; Postma, J. P. M.; van Gunsteren, W. F.; Dinola, A.; Haak, J. R. *J. Chem. Phys.* **1984**, *81*, 3684−3690.
(34) Hou, T. J.; Zhang, W.; Xu, X. J. *J. Phys. Chem. B* **2001**, *105*, 5304−5315.
(35) Zhang, W.; Hou, T. J.; Qiao, X. B.; Huai, S.; Xu, X. J. *J. Mol. Model.* **2004**, *10*, 112−120.
(36) Suarez, D.; Brothers, E. N.; Merz, K. M. *Biochemistry* **2002**, *41*, 6615−6630.
(37) Merz, K. M. *J. Am. Chem. Soc.* **1991**, *113*, 406−411.

(38) Sigfridsson, E.; Ryde, U. *J. Comput. Chem.* **1998**, *19*, 377−395.
(39) Hough, M. A.; Hasnain, S. S. *Structure* **2003**, *11*, 937−946.
(40) Olsson, M. H. M.; Ryde, U.; Roos, B. O.; Pierloot, K. *J. Biol. Inorg. Chem.* **1998**, *3*, 109−125.
(41) Comba, P.; Remenyi, R. *Coord. Chem. Rev.* **2003**, *238*, 9−20.
(42) Schwenk, C. F.; Rode, B. M.; *J. Chem. Phys.* **2003**, *119*, 9523−9531.
(43) Rode, B. M.; Islam, S. M.; Yongyai, Y. *Pure Appl. Chem.* **1991**, *63*, 1725−1732.
(44) Blumberger, J.; Bernasconi, L.; Tavernelli, I.; Vulleumier, R.; Sprik, M. *J. Am. Chem. Soc.* **2004** *126*, 3928−3938.
(45) Falconi, M.; Parrilli, L.; Battistoni, A.; Desideri, A. *Proteins: Struct., Funct., Genet.* **2002**, *47*, 513−520.
(46) Falconi, M.; Brunelli, M.; Pesce, A.; Ferrario, M.; Bolognesi, M.; Desideri, A. *Proteins: Struct., Funct., Genet.* **2003**, *51*, 607−615.
(47) Falconi, M.; Melchionna, S.; Desideri, A. *Biophys. Chem.* **1999**, *81*, 197−205.
(48) Falconi, M.; Venerini, F.; Desideri, A. *Biophys. Chem.* **1998**, *75*, 235−248.
(49) Banci, L.; Carloni, P.; La Penna, G.; Orioli, P. L. *J. Am. Chem. Soc.* **1992**, *114*, 6994−7001.
(50) Banci, L.; Benvenuti, M.; Bertini, I.; Cabelli, D. E.; Calderone, V.; Fantoni, A.; Mangani, S.; Migliardi, M.; Viezzoli, M. S. *J. Am. Chem. Soc.* **2005**, *127*, 13287−13292.
(51) Banci, L.; Bertini, I.; Hallewell, R. A.; Luchinat, C.; Viezzoli, M. S. *Eur. J. Biochem.* **1989**, *184*, 125−129.
(52) Sette, M.; Bozzi, M.; Battistoni, A.; Fasano, M.; Paci, M.; Rotilio, G. *FEBS Lett.* **2000**, *483*, 21−26.
(53) Shen, J.; McCammon, J. A. *Chem. Phys.* **1991**, *158*, 191−198.
(54) Sines, J. J.; McCammon, J. A.; Allison, S. A. *J. Comput. Chem.* **1992**, *13*, 66−69.